American Journal of Applied Sciences 7 (4): 527-534, 2010
ISSN 1546-9239

Analysis of Abnormal Modes of Hoisting DC Electric Drive System

Kosmas Zdrozis
Department of Automation, Technological Educational Institute of Thessaloniki,
P.O. Box 141, Sindos 57400, Greece

Abstract: Problem statement: Host number of publications in which special attention was given to the behavior of the hoisting drives in abnormal modes was found. The effect of the failure of the main power supply on the electrical and mechanical parts of the hoisting drive when the motor is operating in the regenerative braking mode was not enough studied. **Approach:** In this study, the effect of the failure of the main power supply on the electrical and mechanical parts of the hoisting drive when the motor was operating in the regenerative braking mode and give recommendations and solutions to minimize the negative consequences of that abnormal mode. A special comprehensive mathematical mode was developed. The model comprised different submodels that describe the real operation of the power supply, four-quadrant thyristor AC/DC dual converter, firing system, protective devices and mechanism including the elastic elements like ropes and long shafts. This comprehensive model was used to study the behavior of the drive and choose the optimum protective device against the corresponding abnormal mode. **Results:** The failure of the supplying voltage of the dc hoisting drive at power regeneration leads to a significant increase in the motor armature current due to the formed closed loop comprising the armature winding, pair of thyristors and the secondary coil of the supplying transformer, in this mode the converter counter EMF will disappear. The protective device should protect the converter and the motor against such abnormal mode. The produced inrush current in role generates a huge motor torque that result in possible ropes and crane boom deformation, thus the mechanism design should include such possible abnormal mode. **Conclusion:** These results were implemented in the design of a special fast-responding circuit breaker which guarantees the exclusion of the armature current increase in the mentioned mode.

Key words: Hoisting drives, abnormal mode, dual converter, DC motor

INTRODUCTION

Safety and control is crucial in all crane applications. Operating cranes demand precision and leave no margin for errors. The critical starting and stopping can lead to harmful jerks and false tripping, not to mention accidental dropping of the load. Safety for both people and load is of the outmost importance in crane operation.

Optimizing the operation of the crane is also essential. Minimizing cycle time improves productivity. There are also great savings to be made from extended equipment lifetime and more reliable operation without unplanned stops and downtime.

Statement of the problem: Hoisting electric drives are characterized by their ability of operation in braking modes, braking can be dynamic, plugging or regenerative. In modern hoisting electric drives with high hoisting capacity regenerative braking is essential; that is part of the energy stored in the motor can be drawn back to the supply at lowering or speed reduction. The power-electronic converter used in the drive is carefully protected against over-current using fast-responding fuses, the regenerative braking mode is characterized by the high sensitivity to the change in the supplying voltage, which can result in harmful motor current for both DC and AC drives. Other factors like the motor speed and the inductance of the supplying transformer affect the transient character also. Such drives are deeply analyzed and optimally designed for best cranes performance. In (Fox and Collins, 2008) Commutation failure of DC motor drives from voltage sags during regeneration is analyzed, in (Belmans *et al*., 1993). Practical design considerations for braking problems in overhead crane drives are carried out. The use of a DC regenerative motor drive to efficiently provide the charge/discharge capability is proposed in (Jenkins *et al*., 2007). The 4-quadrant DC electric drive with 6-pulse dual converter is modeled in (Zdrozis, 2005); there an attention is given to the regenerative braking mode of the DC hoisting electric

drive. AC drives with regenerative capability and enhanced performance where studied in a host of recent publications; a robust adjustable speed drive with active filtering and regenerative braking capability is proposed in (Gubia *et al*., 2008). High-speed flywheel and motor drive operation for energy recovery in a mobile gantry crane is designed in (Flynn *et al*., 2007). The voltage rise problem due to regenerative braking of DC machines associated with gantry cranes is analyzed in (Lin *et al*., 2007).

MATERIALS AND METHODS

A newly developed converter or control system should be simulated on a computer prior to breadboard or prototype development, particularly if it is complex. The advantages of simulation studies are summarized here. A simulation study can provide the steady-state, transient and fault performance of the system and also can help the design of system and its protection. The software emulation and virtual performance tests give the developer a lot of confidence in the product development. The analysis of waveforms can aid in line power quality studies and design. Simulation results are highly educational. If a simulated system behaves abnormally, there is no fear of any damage. Thus, for DC hoisting drive, the following parts will be simulated as follows.

Separately excited DC motor: For this motor, the field circuit is supplied separately from the armature, as indicated in the Fig. 1. The armature circuit is represented by the series circuit comprising the armature resistance R_a, inductance L_a and the back Electromotive Force (EMF) e_a which is due to the rotation of the armature. The armature current i_a, supplied from the armature voltage supply V_a, develops the torque T_{em}, which is given by (1).

The field circuit, comprising of field resistance R_f and inductance L_f, is supplied from the voltage source V_f. The separately excited DC motor has field coils made with a large number of turns of thin wire, so that the field circuit has a large resistance and carries a small current so that the power loss in field circuit is as small as practicable. Field circuit is not affected by any back EMF.

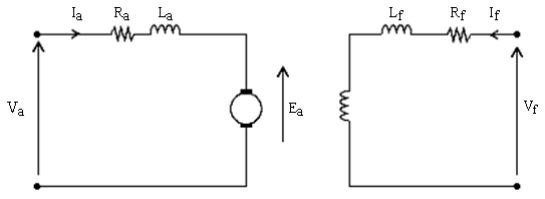

Fig. 1: Equivalent circuit diagram of the DC separately excited motor

In the steady-state, when the supply voltages and speed are constant, the motor currents are DC and the inductance has no voltage across it. Thus, in terms of the DC or average values:

$$V_a = I_a R_a + E_a \tag{1}$$

$$V_a = I_a R_a + K_E' \Phi_f \omega_m \tag{2}$$

and:

$$\omega_m = \frac{V_a - I_a R_a}{K_E' \Phi_f} = \frac{V_a - I_a R_a}{K_E' K_f I_f} \tag{3}$$

also:

$$I_a = \frac{T_{em}}{K_t' \Phi_f} = \frac{T}{K_t' K_f I_f} \tag{4}$$

For full field, $\Phi_{f0} = K_f I_{f0}$.

So that, for full field operation, e.g., for a PM dc motor:

$$I_a = \frac{T_{em}}{K_T} \tag{5}$$

$$\omega_m = \frac{V_a (R_a / K_t' K_f I_f) \times T_{em}}{K_E' K_f I_f} \tag{6}$$

From (3), the possibilities of speed adjustments are via control of V_a or the field current I_f or both. The field variation is normally limited to 0.5-1 p.u., because of commutation requirements. Adjustment of R_a is very inefficient to be effective. Since the armature resistance voltage is normally small, (about 5% of the rated voltage at full load), the adjustment of V_a is the most efficient and effective way of controlling the speed of a DC motor over the full speed range. Speed VS armature voltage characteristic passes through zero, if the brush contact drop is neglected, as indicated in Fig. 2 and 3.

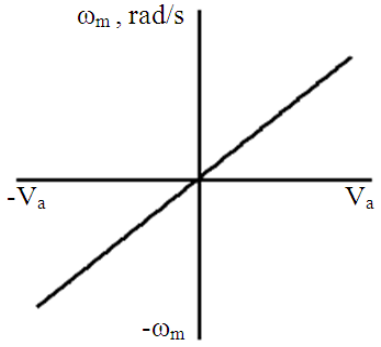

Fig. 2: Motor speed versus armature voltage

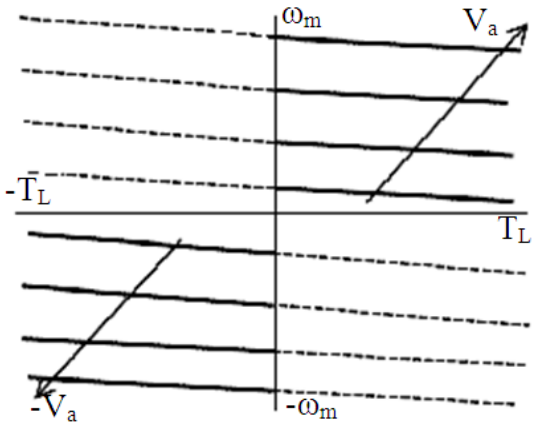

Fig. 3: Speed-torque characteristics with V_a = variable

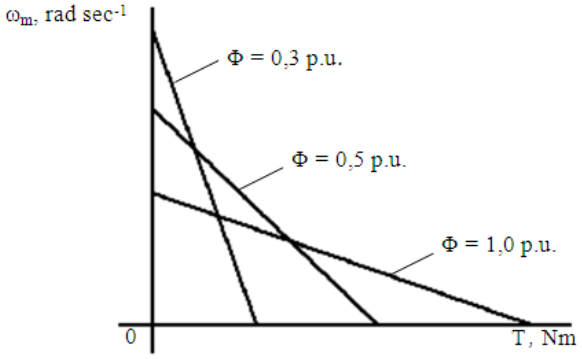

Fig. 4: Speed-torque characteristics with Φ = variable

The speed of the motor drops slightly when the motor is loaded, as indicated in Fig. 4. This drop is due to the effect of the I_aR_a drop, which is small. This assumes that armature reaction is negligible. The motor torque-speed characteristics, as found from the above equations, exist in all four quadrants of the T-ω plane. For V_a = 1 p.u., the motor T-ω characteristic intersects the zero torque axis for a value of torque which is defined as the stall torque of the motor. This can be as high as 20 p.u. torque of the motor for rated field.

From (6) that the motor speed drops more quickly with load torque when the motor field is weaker, as indicated by the Fig. 4.

Thyristor dual converter: The thyristor is perhaps the most efficient and most robust power semiconductor switch. It is a four-layer (3-junction) semiconductor device which can be turned on by a small gate current of a few milliamps. The voltage (and current) ratings of thyristors range from a few tens to several thousands of Volts (Amperes). The thyristor, however, does not gate turn-off capability, at least in its conventional form.

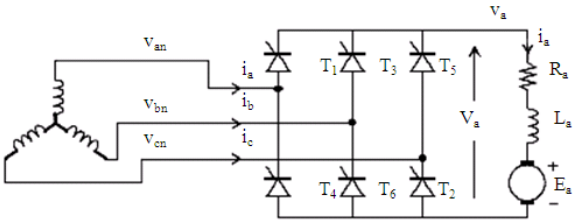

Fig. 5: The power circuit of the separately excited DC motor

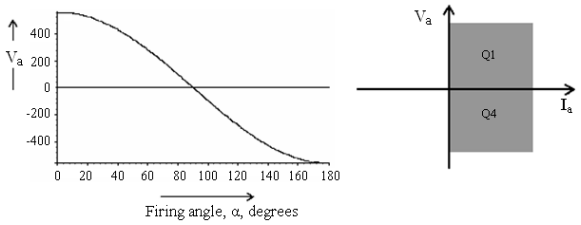

Fig. 6: The armature voltage versus the firing delay angle and the corresponding operating quadrants

The gate turn-off thyristor exists, however, they require special drive gate drive requirements. Once the thyristor is on its anode-cathode voltage is about 1.5 volts and it can then be turned off by removing the gate current and by removing the anode current by some auxiliary or the so-called natural means. The term "natural", also called "natural commutation" refers to thyristor operation in circuits with AC supply. In these circuits, the anode current attempts to reverse due to the nature of the supply voltage, which is of alternate polarity. The thyristor has very good reverse blocking capability and also very good forward blocking capability when its gate current is kept at zero. In this study only conventional, naturally commutated thyristor converters will be considered.

For large DC motor drives, three-phase thyristor converter circuits are preferred due their better output ripple and input harmonic performance. The circuit of the three-phase fully-controlled thyristor bridge converter is shown in Fig. 5.

Analysis of continuous current conduction: The converter average voltage V_d can be determined as follows:

$$V_d = \frac{1}{\pi/3}\int_{\frac{\pi}{3}+\alpha}^{\frac{2\pi}{3}+\alpha} V_{max\,l-l}\sin\omega t\,d(\omega t) = \frac{3V_{max\,l-l}}{\pi}\cos\alpha \qquad (7)$$

This converter operates in quadrants 1 and 4, developing both positive and negative polarity DC

output voltage. For firing angles $0°\leq\alpha\leq90°$, the converter operates in quadrant 1 and for $90°\leq\alpha\leq180°$, the operation is in quadrant 4. Operation in quadrant 4 is of course possible only when the load includes an active DC source, able to source power into the AC circuit (Fig. 6).

From Fourier analysis, the out voltage harmonics for continuous conduction are given by:

$$a_n = \frac{1}{\pi}\int_0^{2\pi} V_{max\,l-l}\cos(n\omega t)d\omega t$$

$$= \frac{3V_{max\,l-l}}{\pi}\left[\frac{2\sin(n+1)\frac{\pi}{6}\cos(n+1)\alpha}{n+1} + \frac{2\sin(n-1)\frac{\pi}{6}\cos(n-1)\alpha}{n-1}\right] \quad (8)$$

$$b_n = \frac{3V_{max\,l-l}}{\pi}\left[\frac{2\sin(n+1)\frac{\pi}{6}\sin(n+1)\alpha}{n+1} + \frac{2\sin(n-1)\frac{\pi}{6}\sin(n-1)\alpha}{n-1}\right] \quad (9)$$

where, n = 6, 12, 18, …

The peak ripple voltage of a harmonic number 6n is given by:

$$C_n = \sqrt{a_n^2 + b_n^2} = \frac{3V_{max\,l-l}}{\pi}\sqrt{\frac{1}{n+1} + \frac{1}{n-1} - \frac{2\cos 2\alpha}{(n-1)(n+1)}} \quad (10)$$

Thus, from the above equations it is seen that three-phase bridge converters circuits have the following attributes, compared to the single- phase bridge converter:

- The output voltage waveform of the converter is smoother, having the lowest harmonic order of six compared to two for the single-phase bridge converter. The ripple voltage to the motor has harmonic order of 6k, where k is any positive integer. The armature current ripple has the same harmonic order. The ripple voltage and currents are also of lower magnitude. The highest output ripple occurs when $\alpha = 90°$
- The lower ripple in the armature current and the smoother voltage waveform calls for smaller armature inductance which may be required to ensure continuous conduction
- The effective converter switching frequency is six times the supply frequency (300 Hz, compared to 100 Hz for a single-phase bridge converter)
- The input current waveform to the converter is closer to being a sinusoid (i.e., better distortion factor), compared to the input current waveform for the single-phase bridge converter. The harmonic order of the AC input line current is given by 6k±1, compared to 2k±1 for the single-phase converter, where k is any positive integer. This calls for reduced filter requirement at the input AC side

The motor current can be exactly determined from the DC and harmonic currents, using DC and AC circuit analysis techniques and then adding the currents for each voltage component. Alternatively, for the interval $\alpha+30° \leq\omega t\leq\alpha+90°$, $V_{max\,l-l}\sin(\omega t + 30°) = i_a R_a + L_a\frac{di_a}{dt} + E_a$, assuming a constant back EMF.

The output voltage waveform repeats every 60°. Solving for i_a:

$$i_a(\omega t) = \frac{V_{max\,l-l}}{|Z_a|}\sin\left(\omega t + \frac{\pi}{6} - \Phi\right) - \frac{E_a}{R_a} + Ae^{-\frac{R_a}{\omega L_a}\left(\omega t - \frac{\pi}{6} - \alpha\right)} \quad (11)$$

The constant of integration A is given by:

$$A = \frac{V_{max\,l-l}\sin(\alpha - \Phi)}{|Z_a|\left(e^{-\frac{R_a}{\omega L_a}\frac{\pi}{3}} - 1\right)} \quad (12)$$

The minimum and maximum armature current values are given by:

$$I_{a\,min} = \frac{V_{max\,l-l}}{|Z_a|}\sin\left(\alpha - \Phi + \frac{\pi}{3}\right) - \frac{E_a}{R_a} + \frac{V_{max\,l-l}}{|Z_a|}\frac{\sin(\alpha - \Phi)e^{-\frac{R_a}{\omega L_a}\frac{\pi}{6}}}{\left(e^{-\frac{R_a}{\omega L_a}\frac{\pi}{3}} - 1\right)} \quad (13)$$

From the complete solution of the armature current, the average and RMS armature current can be determined. For the average armature current, the motor developed torque is found, for the speed for which E_a was used in the calculation. If the conduction is continuous, this is readily shown by the sign of:

$$I_a = \frac{\frac{3V_{max\,l-l}}{\pi}\cos\alpha - E_a}{R_a} \quad (14)$$

Then the average armature current is easily found by (14).

Torque-speed characteristic with continuous conduction: For a given firing angle α, the T-ω characteristics are given by:

$$\omega = \frac{\frac{3V_{max\,l-l}}{\pi}\cos\alpha - I_a R_a - \omega L_{3x} I_a}{K_E} \quad (15)$$

where, L_{3x} is the equivalent source reactance of the three-phase AC source.

Operation in quadrant 1 is for forward driving and operation in quadrant 4 is for reverse (regenerative) braking Fig. 7. The drop in speed with load is partly due to the voltage drop in armature resistance and partly due to the voltage regulation characteristic of the converter as a consequence of the AC side source inductance. The steeper drop in speed indicated by the graphs to the left of the semicircle is due to discontinuous conduction.

As for the single-phase converter, the armature current can become discontinuous, depending on the load, firing angle and motor parameters. The boundary between continuous and discontinuous conduction is found by equating the expression for I_{amin} (13) to zero.

This is indicated by the doted semicircle in the T-ω plane in Fig. 7. The critical inductance for just discontinuous conduction is given by:

$$\frac{R_a}{|Z_a|}\left[\sin\left(\alpha-\Phi+\frac{\pi}{3}\right)+\frac{\sin(\alpha-\Phi)}{e^{-\frac{R_a\pi}{\omega L_a 3}}-1}\right] \geq \frac{E_a}{V_{max\,l-l}} \quad (16)$$

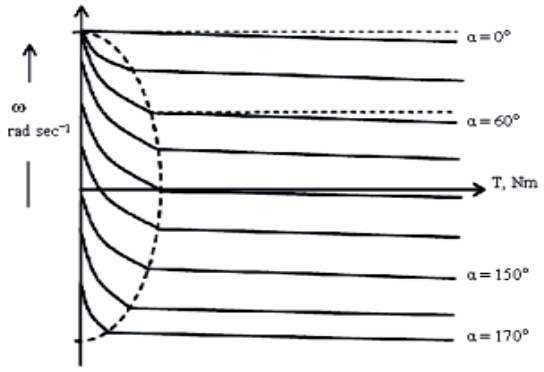

Fig. 7: Speed-torque characteristics including the discontinuous current zone

Analysis of discontinuous current conduction: When the armature current becomes discontinuous, the motor terminal voltage rises to the level of the back EMF, instead of following the AC line-line voltages. The effect is a net increase in the average voltage across the motor and hence speed. If the armature current falls to zero at angle α+γ, where γ is the conduction angle, the solution for the armature current for this condition of operation is found by noting the i_a at α zero in a thyristor is triggered. Thus:

$$0 = \frac{V_{max\,l-l}}{|Z_a|}\sin\left(\alpha-\Phi+\frac{\pi}{3}\right)-\frac{E_a}{R_a}+Ae^{-\frac{R_a}{\omega L_a}\left(-\frac{\pi}{3}\right)} \quad (17)$$

From (11) and (17):

$$i_a = \frac{V_{max\,l-l}}{|Z_a|}\left[\begin{array}{l}\sin\left(\omega t-\Phi+\frac{\pi}{3}\right)-\sin\left(\alpha-\Phi+\frac{\pi}{3}\right)\times \\ e^{-\frac{R_a}{\omega L_a}-\left(\omega t+\frac{\pi}{6}-\alpha\right)}\end{array}\right] - \frac{E_a}{R_a}\left[1-e^{-\frac{R_a}{\omega L_a}-\left(\omega t+\frac{\pi}{6}-\alpha\right)}\right] \quad (18)$$

Current i_a becomes zero at α + γ. Hence:

$$0 = \frac{V_{max\,l-l}}{|Z_a|}\left[\begin{array}{l}\sin\left(\alpha+\gamma-\Phi+\frac{\pi}{3}\right)- \\ \sin\left(\alpha-\Phi+\frac{\pi}{3}\right)\times e^{-\frac{R_a}{\omega L_a}-\left(\gamma+\frac{\pi}{6}\right)}\end{array}\right] - \frac{E_a}{R_a}\left[1-e^{-\frac{R_a}{\omega L_a}-\left(\gamma+\frac{\pi}{6}\right)}\right] \quad (19)$$

The conduction angle γ can be found by solving (19) iteratively. The average and RMS armature current can be found from:

$$I_a = \frac{3}{\pi}\int_{\alpha+\pi/6}^{\alpha+\pi/6+\gamma} i_a d(\omega t) = \frac{3V_{max\,l-l}}{\pi}\left[\begin{array}{l}\cos\left(\alpha+\frac{\pi}{3}\right)- \\ \cos\left(\alpha+\frac{\pi}{3}+\gamma\right)\end{array}\right]+\frac{3E_a}{\pi}\left[\frac{\pi}{3}-\gamma\right] \quad (20)$$

Four-quadrant converter: The three-phase fully-controlled thyristor converter described so far operate in two quadrants, 1 and 4. In order to drive the motor in all four quadrants, two such converters are needed, to be connected back to back as shown in Fig. 8.

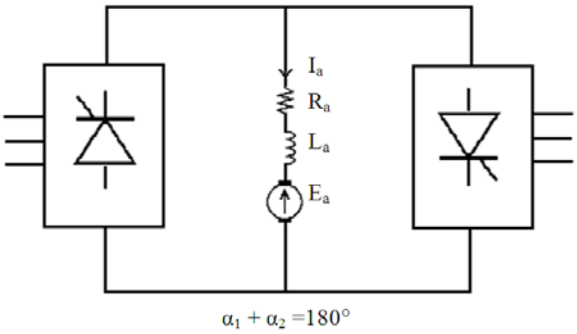

Fig. 8: Thyristor dual converter dc drive

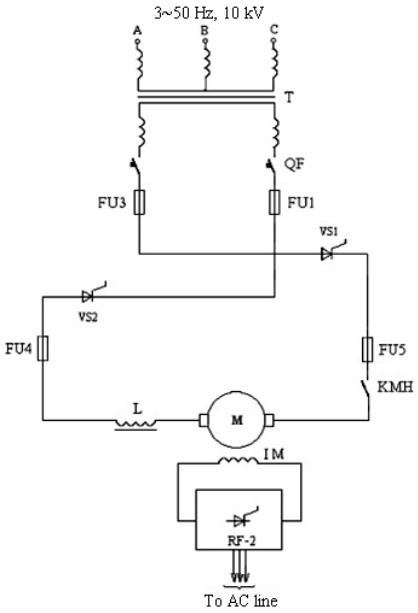

Fig. 9: Equivalent circuit diagram of the armature circuit after voltage failure

RESULTS AND DISCUSSION

Simulation results and qualitative analysis: The mathematical model developed in (Zdrozis, 2005) was used to simulate the process of voltage failure at different lifting and lowering. Specific container crane parameters were used to simulate the following cases:

- Lifting the nominal load (cargo) at the nominal speed
- Lifting light load at the maximum hoisting speed
- Lowering the nominal load at the nominal lowering speed
- Lowering light load at the maximum lowering speed

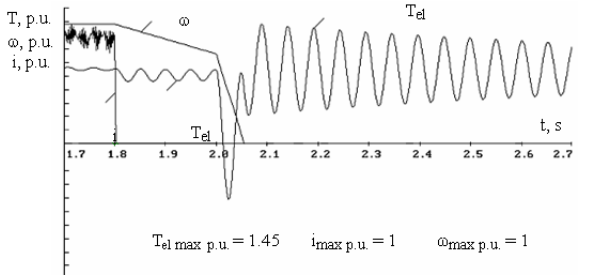

Fig. 10: Voltage failure at lifting the nominal load at the nominal speed

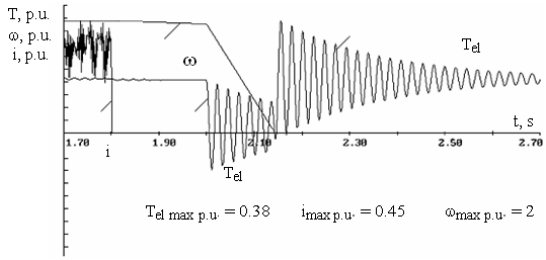

Fig. 11: Voltage failure at lifting light load at the maximum speed

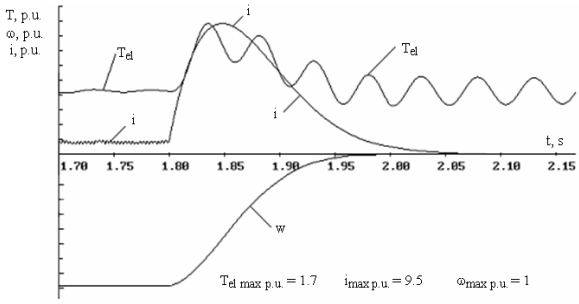

Fig. 12: Voltage failure at lowering the nominal load at the nominal speed without the inclusion of the protecting fuses

In all above mentioned cases, the time at which the voltage failure occurs was assumed to be t = 1.8s. Before this time the drive was operating in the steady-state mode. After 0.2s of the voltage failure the electro-hydraulic brake operates and the drive will be completely stopped.

At the moment of voltage failure the current in the armature circuit will continue flowing via the triggered pair of thyristors of the converter and two secondary windings of the supplying transformer. The equivalent circuit diagram corresponding to the voltage failure mode is shown in Fig. 9.

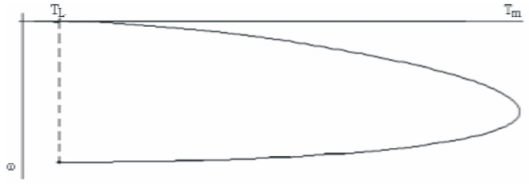

Fig. 13: The dynamic speed-torque characteristic corresponding to Fig. 12

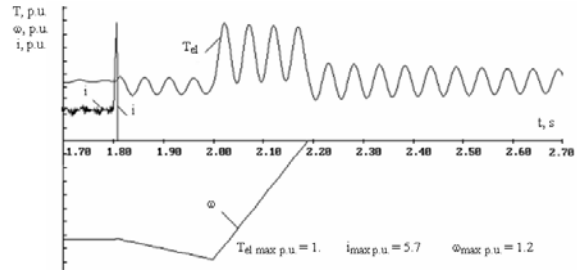

Fig. 14: Voltage failure at lowering the nominal load at the nominal speed including the protecting fuses blowing

Fig. 15: The dynamic speed-torque characteristic corresponding to Fig. 14

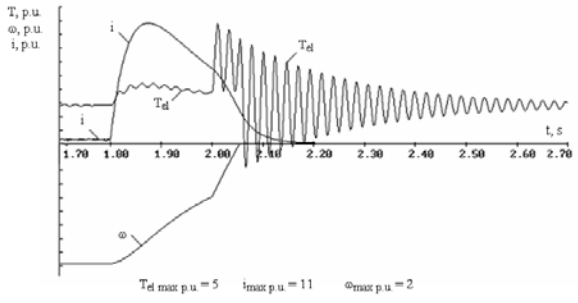

Fig. 16: Voltage failure at lowering a light load at the maximum speed without the inclusion of the protecting fuses

The simulation results for the above mentioned cases are depicted in Fig. 10-19. In Fig. 10-19 the following nomenclatures are used: Motor current-i, the motor speed ω, the elasticity torque T_{el}. The maximum lifting or lowering speed was taken to be twice the rated speed and can be achieved by motor field weakening.

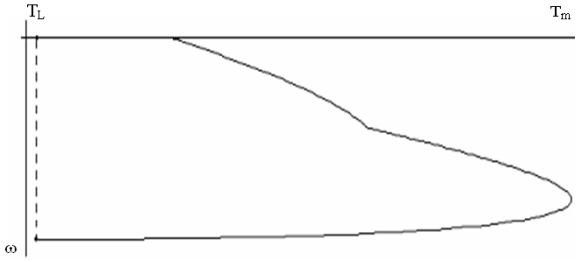

Fig. 17: The dynamic speed-torque characteristic corresponding to Fig. 16

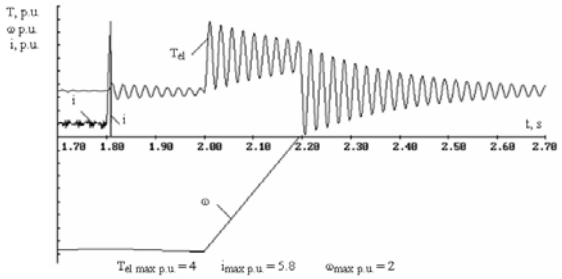

Fig. 18: Voltage failure at lowering a light load at the maximum speed including of the protecting fuses blowing

Fig. 19: The dynamic speed-torque characteristic corresponding to Fig. 18

CONCLUSION

In the present research the abnormal modes of the thyristor dual converter driven DC hoisting drive are investigated. The micro-processes of the supplying voltage sudden failure at lifting and lowering are modeled with a high accuracy. The mathematical analysis and the obtained simulation results revealed that:

- The failure of the supplying voltage at lifting with any speed or at lowering with a speed less than 0.1 of the rated speed does not lead to dangerous consequences neither in the electrical power circuit nor in the mechanical circuit. The mechanical (hydraulic) braking system operates after 0.2s of the voltage failure

- The failure of the supplying voltage at lowering cargos with the nominal or the maximum speed (twice the nominal) is characterized by a huge increase in the armature current, blowing the protecting fuses, decreasing the lifetime of the windings insulation and the crane ropes are exposed to strong torsional vibrations due to the high increase in the motor braking torque
- Installing an automatic circuit breaker in the armature circuit with a total switching-off time up to 2ms significantly decreases the dangerous consequences caused by the failure of the supplying voltage at lowering cargos, increases the reliability of the crane operation, cancels the money waste due to replacing the power fuses and the crane complete shutdown-time taken for blown fuses replacement

REFERENCES

Belmans R., F. Busschots and R. Timmer, 1993. Practical design considerations for braking problems in overhead crane drives. Proceeding of the IEEE Conference Industry Applications Society Annual Meeting, Oct. 2-8, IEEE Xplore Press, Toronto, Ont., pp: 473-479. DOI: 10.1109/IAS.1993298966

Flynn, M.M., P. McMullen and O. Solis, 2007. High-speed flywheel and motor drive operation for energy recovery in a mobile gantry crane. Proceeding of the 22nd IEEE Annual Conference on Applied Power Electronics, (APE'07), IEEE Xplore Press, USA., pp: 1151-1157. DOI: 10.1109/APEX.2007.357660

Fox, J.C. and E.R. Collins, 2008. Commutation failure of dc motor drives from voltage sags during regeneration. Proceeding of the IEEE 13th International Conference on Harmonics and Quality of Power, Sept. 28-Oct. 1, IEEE Xplore Press, Wollongong, NSW., pp: 1-9. DOI: 10.1109/ICHQP.2008.4668867

Gubia, E., P. Sanchis, J. Lopez, A. Ursua and L. Marroyo, 2008. Robust adjustable speed drive with active filtering and regenerative braking capability. Proceeding of the IEEE 34th Annual Conference on Industrial Electronics, Nov. 10-13, IEEE Xplore Press, Orlando FL., pp: 938-941. DOI: 10.1109/IECON.2008.4758079

Jenkins, J.E., H.P. Jenkins, T. Piekarski and M. Waller, 2007. DC regenerative drive use for battery charge/discharge cycling. Proceeding of the IEEE Southeast Conference, (SC'07), IEEE Xplore Press, USA., pp: 478-482. DOI: 10.1109/SECON.2007.342948

Lin, Y.J., C.Y. Hung and T.C. Hung, 2007. Voltage Rise due to regenerative braking of DC machines associated with gantry cranes at Kaohsiung Harbor. Proceeding of the IEEE Conference on Electrical Power, Oct. 25-26, IEEE Xplore Press, Montreal, Canada, pp: 452-455. DOI: 10.1109/EPC.2007.4520374

Zdrozis, K., 2005. Mathematical model of 4-quadrant DC electric drive with 6-pulse dual converter. Am. J. Applied Sci., 2: 1025-1027. http://www.scipub.org/fulltext/ajas/ajas251025-1027.pdf